Climate change effects on submarine groundwater discharge and regional variations along the Korean Peninsula

Hahn Chul Jung[1], Yeosang Yoon[2,3,*]

[1] Department of Earth System Sciences, Yonsei University, Seoul, South Korea
[2] Hydrological Sciences Laboratory, NASA Goddard Space Flight Center, Greenbelt, MD, USA
[3] Science Applications International Corporation, Reston, VA, USA

[*] Corresponding author. Code 617, Hydrological Sciences Laboratory, NASA Goddard Space Flight Center, Greenbelt, MD 20771, USA. Email: yeosang.yoon@nasa.gov

Hahn Chul Jung and Yeosang Yoon: These authors contributed equally.

Abstract

Climate change impacts fresh submarine groundwater discharge on the Korean Peninsula, increasing the vulnerability of coastal regions to environmental degradation and economic consequences. Here, we provide regional estimates of fresh submarine groundwater discharge along the entire coast using established water balance methods. Our findings reveal that the western and southern coasts of the southern Korean Peninsula exhibit higher fresh submarine groundwater discharge rates due to greater net precipitation compared to the northern Korean Peninsula. Differences in drainage length between the east and west coasts, along with substantial tidal flats, significantly influence submarine groundwater discharge rates. Climate change drives variations in fresh submarine groundwater discharge, with rising trends in the southern Korean Peninsula during spring and winter, while the northern coastal watersheds show consistent increases across all seasons. Coastal vulnerability to offshore contamination from land use development affects 15% of the coastline. Notably, between 1990 and 2020, the risk in the southern Korean Peninsula's coastal catchments increased by 38%. Our analysis also highlights heightened vulnerability to saltwater intrusion in the southwestern Korean Peninsula.

Introduction

Submarine groundwater discharge (SGD) represents the subsurface flow of water entering the ocean[1,2]. SGD impacts the coastal environment in various ways, depending on factors such as discharge scale, groundwater quality, and human proximity to the discharge zone[3]. Instances of SGD can lead to saltwater intrusion into coastal aquifers, posing potential threats. The compromised water quality associated with SGD, characterized by pollutant loading or harmful algal blooms, can negatively affect both human health and the environment[4,5]. Additionally, tidal or wave setup can influence the replenishment of coastal aquifers with seawater during flood tides[6]. On the Korean Peninsula, groundwater extraction for agricultural, industrial, and domestic purposes is increasing, potentially impacting the SGD process in coastal aquifers[7,8,9].

Quantifying SGD estimates and examining their spatiotemporal variability are crucial. At a local scale, common field techniques for assessing of fresh SGD include seepage meters[10,11,12], piezometers[13], and the use of natural tracers such as radium and radon[14,15,16]. However, direct measurements are limited by spatial coverage constraints, posing significant challenges in quantifying fresh SGD due to its high heterogeneity. Computational methods provide a valuable tool for predicting fresh SGD at various spatial scales, from global (e.g., ref. 17,18,19) to regional perspectives (e.g., ref. 20,21,22). The southern Korean Peninsula has been actively involved in calculating both local and regional SGD estimates, utilizing both direct seepage measurements and indirect isotopic methods[9,16,23,24,25]. However, there has been no attempt to estimate fresh SGD along the entire Korean Peninsula coast using the water balance approach in combination with advanced land surface models (LSMs). Previous studies have applied LSMs to estimate SGD using the Global Land Data Assimilation System (GLDAS) to calculate water budgets for coastal aquifers and approximate net recharge rates on a coarse resolution[17,18,22]. GLDAS provides products related to infiltrating runoff from various LSMs and meteorological forcing datasets in near real-time. GLDAS version 1 offers a spatial resolution of 1 degree, while version 2 provides an improved resolution of 0.25 degree[26]. Despite the improvements, GLDAS still struggles to capture the complex topography of coastal regions due to spatial limitations when applied to the Korean Peninsula. Previous assessments of fresh SGD have primarily focused on long-term averages, failing to provide insights into the temporal evolution of fresh SGD rates or assess the impact of climate change on SGD variations across coastal catchments[17,18]. Note that coastal catchments are the land areas directing water flow towards the coast, rather than to stream. Recently, the Korea Land Data Assimilation System (KLDAS) has been developed within the NASA Land Information System framework[27], benefiting from the incorporation of local precipitation forcing datasets and soil texture maps[28,29]. The KLDAS supports an effective hydrological monitoring system by providing continuous high-resolution (i.e., 0.01 degree) water balance variables across the Korean Peninsula.

This study focuses on fresh SGD originating onshore, which is distinct from saline groundwater circulating through the seabed. While the understanding of fresh SGD fluxes remains incomplete, these fluxes are influenced by geological factors, topography, climate, and land use[30]. Therefore, we undertake a comprehensive analysis focusing on four key aspects. Firstly, we quantify fresh SGD rates along the entire coast of the Korean Peninsula using a water balance approach through KLDAS for the period 1980-2016. We investigate the spatial pattern of average fresh SGD rates, considering factors such as net precipitation and coastal drainage length across regions. Secondly,

we assess the influence of climate change on fresh SGD rate variations over a 37-year model period. We analyze annual and seasonal trends using the Mann-Kendall trend test. Thirdly, we examine the susceptibility of coastal areas in the southern Korean Peninsula to offshore contamination and saltwater intrusion, accounting for land use development over decades. Finally, we explore terrestrial water storage anomalies over coastal catchments using Gravity Recovery and Climate Experiment (GRACE) satellite products to evaluate the coastal vulnerability of the Korean Peninsula.

Results and Discussion

Regional analysis of fresh SGD rates

The Korean Peninsula includes numerous small islands, primarily located to the west and south, which account for 43.6% of the total number of coastal catchments. Despite their substantial count, the SGD from these minor islands remains relatively small across all regions due to their limited drainage lengths (Supplementary Fig. 1). To prevent statistical biases, these minor islands are excluded from the analysis (Fig. 1). The topography of the Korean Peninsula significantly influences its annual rainfall patterns. The southwestern region, positioned on the windward side of high mountains, receives abundant rainfall, while the northeastern region, surrounded by mountains, experiences lower precipitation levels (Supplementary Fig. 1b). Drainage length, representing the average distance from any location in the coastal catchment to the shoreline, tends to be smaller in the southwestern region with small-sized islands (Supplementary Fig. 1c).

Three LSMs–Noah v3.9[31,32], Noah-Multi Parameterization (Noah-MP) v4.0.1[33,34], and Joint UK Land Environment Simulator (JULES) v5.5[35,36]–were employed to calculate water budgets for coastal aquifers and estimate fresh SGD along the Korean Peninsula. These models incorporate diverse parameterizations and physics, enhancing robustness by reducing biases and improving uncertainty assessment[37]. The ensemble average fresh SGD for the entire domain was determined to be 279 m^2/year, with an uncertainty of 16.3 m^2/year (Table 1). Uncertainty varies significantly across regions, with higher values in Gyeongnam, Pyongan, and Hamgyong, while Chungnam, Jeju, and Gyeongbuk exhibit more consistent predictions. Factors contributing to uncertainty include model structure and parameterization. Variations in soil moisture dynamics and groundwater flow among LSMs further propagate regional uncertainty. Assumptions about aquifer connectivity and subsurface properties also affect accuracy, underscoring the need for future refinements in regional-scale SGD assessments.

We compared our estimated fresh SGD with previous studies[7,18,19], employing different approaches. Ref. 18 reported ensemble average SGD rates of 264 m^2/year for the Korean Peninsula using a similar water balance method, aligning well with our findings. This estimate was recalculated by isolating the Korean Peninsula domain and excluding coastal catchment areas smaller than 1 km^2. Ref. 19 applied a global numerical groundwater model, yielding an average SGD rate of 94 m^2/year for the Korean Peninsula, with a range of 1–696 m^2/year based on 130 sensitivity model runs. These estimates, recalculated for the Korean Peninsula domain, exhibit larger uncertainties due to factors such as topography, permeability, recharge, and contributing area size, encompassing the range of our estimates. Ref. 7 used 155 local field measurements combined with Darcy's law, reporting median SGD rates of 292 m^2/year for the Chungnam, 657 m^2/year for Jeolla, 949 m^2/year for the Gyeongnam and Gyeongbuk. Most of our estimated SGD values are lower, likely because field

measurements often overestimate fresh SGD by targeting areas with concentrated discharge, such as permeable sands or bay heads[17]. Additionally, local measurements may not represent regional-scale due to the high spatial heterogeneity of fresh SGD.

The patterns of fresh SGD are influenced by a combination of drainage geometry and climate conditions (Fig. 2 and Table 1), consistent with Eq. (1). Note that, among the meteorological inputs driving the LSMs, precipitation is the most significant factor contributing to the recharge rate[38,39]. Net precipitation is used instead of total precipitation to better illustrate the relationship between fresh SGD and climate conditions. In the northern Korean Peninsula region, including areas like Pyongan, Hwangnam, and Hamgyong, both net precipitation and fresh SGD exhibit lower values. Conversely, the western and southern coasts of the southern Korean Peninsula experience higher levels of net precipitation and fresh SGD. The impact of drainage length becomes apparent when examining the east and west coasts. For instance, net precipitation levels are similar in the Chungman and Gangwon regions, but fresh SGD rates are approximately 47% greater in the Chungman region. This disparity can be attributed to the presence of extensive coastal drainage systems within complex terrains. Substantial tidal flats are present along the west coast, where tidal differences play a crucial role in influencing high SGD rates[8]. Additionally, the west coast is predominantly composed of sandy tidal flats, which can increase fresh SGD rates. The nutrient runoff via groundwater on large continental shelves affects potential ecological systems and needs continuous monitoring. Jeju Island exhibits notably high fresh SGD rate of 415 m^2/year, exceeding the 157 m^2/year observed along the coastal shorelines of Oahu Island, Hawaii, as estimated using the MODFLOW groundwater model under steady-state conditions[40]. While both islands share a volcanic origin, their geological histories differ significantly. Groundwater on Jeju Island originates from volcanic rock aquifers, primarily consisting of permeable basalts. The island's significant elevation changes, permeable volcanic bedrock, and limited river drainage infrastructure collectively contribute to its elevated SGD rates. This is particularly critical as groundwater contamination profoundly impacts coastal ecosystems and contributes to eutrophication.

Impact of climate change on the fresh SGD rates

SGD exhibits a rising trend across the entirety of the Korean Peninsula (Fig. 3a). This pattern aligns with the observed trend in net precipitation (Fig. 3b). Most regions in the southern Korean Peninsula do not display statistically significant trends, either increasing or decreasing. However, discernible statistically significant trends are evident in the Gyeonggi region and various areas within the northern Korean Peninsula.

Seasonal variations in fresh SGD rates (Figs. 4a-4d) closely follow precipitation patterns, with most of the rainfall occurring during the summer months. Positioned within the temperate monsoon climate zone, the Korean Peninsula distinctly experiences the seasons of spring, summer, autumn, and winter. Spring and autumn are marked by clear and dry weather influenced by migratory high-pressure systems, while summer sees hot and humid conditions due to the impact of the North Pacific high-pressure system. Conversely, winter is characterized by cold and dry conditions influenced by the continental high-pressure system. Notably, during the summer season, rainfall constitutes 54% of the annual precipitation. This discernible trend is most conspicuous in the watersheds along the western and southern coasts of the Korean Peninsula during the summer (Fig. 4b). Conversely, watersheds along the eastern coast

consistently exhibit low SGD rates throughout all seasons. The primary contributing factor to this phenomenon is the higher relative rainfall observed on the western and southern coasts compared to the eastern coast. Furthermore, the intricate coastline features in the western and southern seas, characterized by longer drainage lengths, make fresh SGD rates highly responsive to variations in precipitation. Examining the seasonal trends of fresh SGD rates (Figs. 4e-4h), notable distinctions between the southern and northern Korean Peninsula become apparent. Coastal watersheds in the northern Korean Peninsula show a consistent trend of increasing fresh SGD rates across all seasons. In contrast, regions of the southern Korean Peninsula, including the western and southern coasts and Jeju Island, distinctly exhibit rising trends in fresh SGD during both the spring (Fig. 4e) and winter (Fig. 4h), while trends observed during the summer (Fig. 4f) and fall (Fig. 4g) are subdued. The spring season is affected by climate change, resulting in increased rainfall in these areas. Moreover, reduced soil moisture freezing (i.e., increased infiltration) due to rising winter temperatures leads to increased aquifer recharge.

While this study focuses on long-term trends, we acknowledge that short-term climate events, such as typhoons and extreme precipitation, also significantly influence fresh SGD. These events can increase salinity due to sea level rise and reduce fresh SGD through rapid runoff, particularly in regions with smaller drainage basins, and should be considered in future studies.

Impact of decadal land use changes on coastal vulnerability

Fresh SGD estimates also reveal potential contamination threats to the ocean and fisheries, upon which coastal populations heavily rely (Fig. 5a). Our definition of vulnerability generally holds true when increases in onshore aquifer contaminant concentrations coincide with a higher fraction of developed land and when the coastal supply rate correlates with elevated fresh SGD rates. Coastal areas with above-average fresh SGD and land development are particularly vulnerable to groundwater-borne contamination, accounting for 15% of the entire coastline (Fig 5a). Vulnerable regions include the western and southern parts of the Korean Peninsula. Notably, almost all of the coastal catchments in the Jeju Island area are susceptible to contamination. According to the Land Cover Change Map between 1980 and 2010 from the Ministry of Environment of South Korea (https://egis.me.go.kr), developed and agricultural lands increased by 2% and 24%, respectively, in the Jeju Island area, which is situated along the coastline. This developmental expansion contributes to elevated nutrient loads in the groundwater. Given that Jeju Island is a volcanic island and heavily relies on groundwater for its water resources, and considering that a majority of its population resides along the coast, addressing this issue is crucial. The reliance of drinking water, agriculture, and industrial activities on freshwater derived from underground sources and surface runoff underscores the need for continuous monitoring of nutrient inputs from fresh SGD[25].

Fig. 5a also illustrates the vulnerability of coastal aquifers to saltwater intrusion. Saltwater intrusion can occur in areas where groundwater is discharged into the ocean through underground conduits as part of SGD. Vulnerability to saltwater intrusion is particularly high in the southwest regions (i.e., Jeolla and Gyeongnam) (Fig. 5a). Coastal aquifers in these areas cannot be directly used for agriculture, such as cultivating salt-sensitive crops. These regions are especially susceptible to excessive groundwater extraction and salinity damage during droughts caused by climate change.

This vulnerability is further supported by the 2022 Marine Infiltration Survey Report from the Korea Rural Community Corporation (https://www.groundwater.or.kr), which analyzed data from 225 in-situ monitoring gauges across the southern Korean Peninsula. The report indicates that 31% of the gauges show a continuous decline in coastal aquifer levels, indicating excessive groundwater extraction, while 38% demonstrate a sustained increase in electrical conductivity, suggesting salinity intrusion. Furthermore, ongoing global warming trends contribute to a consistent rise in sea levels, which poses additional challenges to coastal lowland agricultural areas, such as an increasing risk of flooding and saltwater intrusion. The Korea Hydrographic and Oceanographic Agency (www.khoa.go.kr) conducted an analysis of sea level height data gathered from 21 coastal tide gauging stations. The findings also indicate that over the past 34 years (1989 to 2022), the sea level along the Korean coast has experienced a rise at a rate of 3.03 mm/year, culminating in a total average increase of approximately 10.3 cm. In Jeju Island, both the western and eastern regions are vulnerable to offshore contamination and saltwater intrusion. As mentioned earlier, these areas rely primarily on groundwater to meet their resource demands. If groundwater extraction reduces fresh SGD below a critical threshold, salinization can occur[41].

Fig. 5b illustrates the changes in developed and agricultural land in the southern Korean Peninsula's coastal catchments since 1990 and their corresponding impact on vulnerability to offshore contamination. Note that the northern Korean Peninsula region was excluded from the study due to limited access to datasets. The overall proportion of developed and agricultural land has consistently increased from 1990 to 2020 due to economic growth, population expansion, and shifts in cultivated crops. Specifically, the developed area has expanded rapidly by 6.8%, while agricultural land has gradually declined by 4%. These changes have exacerbated the vulnerability of offshore contamination-prone regions by 38% since 1990 with the issue notably concentrated in the western and southern coastal regions.

The analysis of GRACE total water storage (TWS) anomalies[42] also reveals a decreasing pattern of groundwater across coastal catchments. Fig. 6 depicts the anomalies in TWS (mm) over coastal catchments from GRACE during 2002–2016, along with their piecewise linear trends. TWS represents an integrated measure of the terrestrial water budget, encompassing groundwater, soil moisture, surface water, ice, snow, and water in vegetation. While TWS does not directly measure groundwater storage, changes in groundwater storage trends can be identified through TWS fluctuations. Coastal catchments do not contain streams, and TWS is more similar to groundwater storage compared to non-coastal catchments. The figure indicates no significant change until 2011, but from 2011 to 2016, a notable depletion of TWS (-0.79 mm/month) is evident. This issue primarily arises as domestic agriculture shifts towards high-value facility farming, leading to increased groundwater usage in these coastal areas. Note that groundwater levels decrease due to reduced recharge or increased extraction, which can lead to a reduction in SGD. Additionally, lower groundwater levels can heighten the risk of saltwater intrusion into coastal aquifers, leading to the contamination of freshwater resources with saline water.

Conclusions

This study addresses the susceptibility of the Korean coastal environment to vulnerability due to SGD. We present the first regional estimates of fresh SGD along

the entire coast of the Korean Peninsula from 1980 to 2016. The ensemble average for the entire domain was found to be 279 m^2/year, with the uncertainty in fresh SGD estimated at 16.3 m^2/year. In the northern Korean Peninsula region, fresh SGD exhibit lower values on average 203 m^2/year with lower net precipitation than 500 mm/year, although overall its drainage lengths are longer than the southern Korean Peninsula. For the southern Korean Peninsula region, Chungnam shows the highest SGD rates (486 m^2/year) where it is located on the west sea, experiencing the world's most significant tidal differences and featuring extensive tidal flats. Jeju and Gyeongnam also show higher SGD rates than 400 m^2/year with combined high net precipitation and high drainage length. Additionally, regions of the southern Korean Peninsula exhibit distinct rising trends in fresh SGD during both the spring and winter seasons. Climate change has led to increased spring rainfall in these southern Korean Peninsula regions. Rising winter temperatures reduce soil moisture freezing, resulting in greater surface and subsurface water inflow. From 1990 to 2020, economic growth and population expansion in the southern Korean Peninsula's coastal catchments have led to increased vulnerability to groundwater-borne contamination across coastal areas, affecting 15% of the entire coastline. During this period, developed areas have expanded by 6%, while agricultural land has decreased by 4%. These land use changes have heightened the susceptibility of regions prone to offshore contamination by 38% over the past 30 years, with the western and southern coastal regions being particularly affected.

The outcomes of this research provide a fundamental foundation and support for a nationwide coastal vulnerability monitoring system. Our regional LSMs enable the continuous assessment of regional recharge rates and provide land-derived SGD rates along the coast of the Korean Peninsula. To enhance the accuracy of SGD rates using LSM approaches, it is essential to integrate local meteorological forcing datasets and land surface parameters into our regional LSM. This integration will help derive hydrologic variables relevant to SGD and allow for more precise topography for improved delineation of coastal catchments. Our water budget analysis does not account for hydraulic head gradients, which are typically necessary for local groundwater numerical modeling. Given that steeper hydraulic head gradients in coastal areas can drive higher rates of fresh SGD, hydraulic head is a critical factor influencing fresh SGD flow in these regions. For future studies, integrating our ensemble land surface models with numerical groundwater modeling would be beneficial for estimating fresh SGD rates at more localized scales. Additionally, the thermal infrared sensors of optical satellite missions can resolve the spatial variation of SGD rates and detect potential groundwater discharge areas along the coast of the Korean Peninsula[43].

Methods

Estimation of fresh SGD

Coastal catchments for fresh SGD were identified using the HydroSHED 15-arc second product (https://www.hydrosheds.org/). These catchments are intentionally designed to exclude streams and are instead located between established points where streams meet the coast. The coastlines were delineated through the extraction of polyline products utilizing feature type attributes.

We derive the adjusted net recharge rate for each coastal catchment by averaging the infiltrating runoff, taking into account soil properties, land cover types, and evapotranspiration loss from three LSMs: Noah v3.9, Noah-MP v4.0.1, and JULES

v5.5. Model parameters, forcings, and the overall model setup were obtained from ref. 28. Specifically, the LSMs were run using a 15-minute timestep over a 37-year period (1980 – 2016) at a spatial resolution of 0.01 degrees[28,29]. The initial conditions for the simulation were established by running the LSMs from 1980 to 2016 twice, followed by a reinitialization in 1980. KLDAS was used as a driving force for the LSMs. The KLDAS encompasses the entirety of the Korean Peninsula, spanning from 33 to 44 degrees north and 124 to 132 degrees east. The KLDAS operates at a spatial resolution of 0.01 degrees, incorporating local precipitation forcing datasets and soil texture maps. The high-resolution elevation data from Multi-Error-Removed Improved-Terrain datasets at 3-arc second resolution (~ 90 m)[44] is used to derive the topography dataset of elevation, slope, and aspect. All LSMs integrations use the modified International Geosphere Biosphere Programme Moderate Resolution Imaging Spectroradiometer (MODIS) 20-category landuse data[45] and the soils data from the International Soil Reference and Information Centre[46]. The annual recharge volume for each coastal catchment (m^3/year) was calculated by multiplying the catchment area (A; m^2) by the annual recharge (r; m/year) closest to the catchment centroid. Finally, to derive the fresh SGD flux (m^2/year), the annual recharge volume was divided by the corresponding coastline length (L; m), following ref. 17 and 18:

$$SGD\ (m^2/year) = r\ (m/year) \times A\ (m^2) / L\ (m) \quad (1)$$

where, A/L is referred to as the drainage length (m).

We simplify our calculations by excluding groundwater contributions from upland catchments to coastal catchments, which may lead underestimation of fresh SGD. Additionally, human activities such as groundwater pumping (e.g., for irrigation and urban water supply) are neglected, which can lead to high estimates. For the correlation analysis, we also calculated net precipitation as rainfall minus evapotranspiration, which were estimated from LSMs. The uncertainty of SGD is calculated as the standard deviation of estimates from the three LSMs. Note that details of LSM performance based on parameters and meteorological forcings are not presented in this study but can be found in ref. 28.

Mann-Kendal trend test

The Mann-Kendall test, a non-parametric technique applied to evaluate monotonic trends in environmental datasets such as climate or hydrological data[47], employs the S statistic to determine the existence and extent of upward or downward patterns observed over time:

$$S = \sum_{k=1}^{n-1} \sum_{j=k+1}^{n} sign(x_j - x_k) \quad (2)$$

where x represents the time series variable, with subscripts j and k denoting observation times. The $sign(x_j - x_k)$ function yields values of +1, 0, or -1, indicating increasing, no, and decreasing trends, respectively. The S values are scaled to a range of [-1, 1] for improved interpretability. The null hypothesis posits that there is no statistically significant trend in the data, with significance set at a level of 5% (or 95% confidence level).

Estimation of coastal vulnerability to offshore contamination

Following the ref. 17, we classified coastlines as susceptible to groundwater contamination when the proportion of developed and agricultural land surpassed the average (38.7%) and the fresh SGD flux exceeded the average (279 m^2/year). Our vulnerability criteria generally apply if onshore aquifer contaminant concentrations increase alongside the fraction of developed land, and if coastal supply rates rise with fresh SGD rates, although multiple factors can influence contaminant flux to the coast.

To determine the percentage of developed and agricultural land in the southern Korean Peninsula's coastal catchments, we utilized the 2010 Land Cover Map from the Ministry of Environment of South Korea (https://egis.me.go.kr), which categorizes land into seven major types at a 30-meter resolution. For the northern Korean Peninsula, we extracted land fraction data using the MODIS Land Cover Type (MCD12Q1) V6.1 2010 dataset[48]. The MODIS MCD12Q1 provides annual global land cover maps at a 500-meter resolution from 2001 to the present. We converted the raster data to a polygon shapefile and calculated the total areas of developed and crop land within each catchment.

Estimation of coastal vulnerability to saltwater intrusion

To assess vulnerability to saltwater intrusion in the southern Korean Peninsula, with the exception of Jeju, we utilized data from the 2010 Marine Infiltration Survey Report, compiled by the Korea Rural Community Corporation (https://www.groundwater.or.kr). This report relied on data collected from 107 in-situ gauges and categorized vulnerability into four stages (interest, attention, caution, and serious) based on parameters such as electrical conductivity, its variations, and changes in reservoir levels. We identified and classified the coastal catchments as vulnerable to saltwater intrusion when the report categorized them as being in caution and serious stages. Similarly, for the Jeju Island region, we sourced information from the 2022 Groundwater Monitoring Report, prepared by the Jeju Groundwater Research Center (https://water.jeju.go.kr). Note that we did not assess the vulnerability to saltwater intrusion in the northern Korean Peninsula due to limited available data, and the in-situ gauges do not cover all coastal catchments in the southern Korean Peninsula.

Impact of decadal land use changes on coastal vulnerability to offshore contamination

To evaluate the proportion of developed and agricultural land in the southern Korean Peninsula's coastal catchments over time, we analyzed four sequential datasets (1990, 2000, 2010, and 2020) from the Land Cover Map (Fig. 5b) provided by the Ministry of Environment of South Korea (https://egis.me.go.kr). This methodology is similar to the approach used for assessing offshore contamination vulnerability, as detailed in ref. 17. We established specific thresholds for averaged fresh SGD flux corresponding to the year of SGD estimation. However, due to the study's timeframe, the 2020 data was beyond our scope. To address this, we utilized the 2012 SGD estimates as a proxy for the 2020 estimates, given the similarity in precipitation patterns and spatial distribution between 2012 and 2020.

TWS anomalies over the coastal catchment

We utilize three distinct GRACE products, which are provided monthly on 1-degree horizontal resolution grids by the University of Texas Center for Space Research, Jet Propulsion Laboratory, and German Research Centre for Geosciences. These products are derived from the RL06v04 spherical harmonics fields[49]. To extract TWS anomalies

over the coastal catchments, we interpolated the GRACE datasets to fit the 1-km LSM grid and extracted the value closest to the catchment centroid.

Data availability

HydroSHED 15-arc second products were downloaded from the HydroSHED website (https://www.hydrosheds.org/). The land cover map for the southern Korean Peninsula was downloaded from the Ministry of Environment of South Korea (https://egis.me.go.kr). The MODIS MCD12Q1 V6.1 was obtained from the Land Processes Distributed Active Archive Center (https://lpdaac.usgs.gov/products/mcd12q1v061/). Gauge datasets for saltwater intrusion in the southern Korean Peninsula are available from the Korea Rural Community Corporation (https://www.groundwater.or.kr). Saltwater intrusion observations for Jeju can be found at the Jeju Groundwater Research Center (https://water.jeju.go.kr). GRACE datasets were downloaded from NASA JPL GRACE Tellus (https://grace.jpl.nasa.gov).

Code availability

The three LSMs (Noah v3.9, Noah-MP v4.0.1, and JULES v5.5) are available via the NASA Land Information System (https://github.com/NASA-LIS/LISF).

References

1. Burnett, W. C., Aggarwal, P. K., Aureli, A., Bokuniewicz, H., Cable, J. E., Charette, M. A., et al. Quantifying submarine groundwater discharge in the coastal zone via multiple methods. *Sci. Total Environ.* **367**, 2-3, 498–543 (2006).
2. Michael, H. A., Russoniello, C. J. & Byron, L. A. Global assessment of vulnerability to sea-level rise in topography-limited and recharge limited coastal groundwater systems. *Water Resour. Res.* **49**, 2228–2240 (2013).
3. Lecher, A. L. & Mackey, K. R. M. Synthesizing the effects of submarine groundwater discharge on marine biota. *Hydrol.*, **5**, 4, 60 (2018).
4. Knee, K. L., & Paytan, A. Submarine groundwater discharge: A source of nutrients, metals, and pollutants to the coastal ocean. *Treatise on Estuarine and Coastal Science*, **4**, 205–233 (2012).
5. Hu, C., Muller-Karger, F. E., & Swarzenski, P. W. Hurricanes, submarine groundwater discharge, and Florida's red tides. *Geophys. Res. Lett*. **33**, 11 (2006)
6. Nielsen, P. Tidal dynamics of the water table in beaches. *Water Resour. Res.* **26**, 9, 2127–2134 (1990).
7. Han, S.-Y., Hong, S.-H. & Park, N. Distribution of coastal ground water discharge from surficial aquifers of major river districts. *KSCE J. Civ. Eng.* **26**, 1-6 (2006).
8. Kim, G., Ryu, J.-W., Yang, H.-S. & Yun, S.-T. Submarine groundwater discharge (SGD) into the Yellow Sea revealed by 228Ra and 226Ra isotopes: implications for global silicate fluxes. *Earth Planet Sci. Lett.* **237**, 156–166 (2005).
9. Hwang, D.-W., Kim, G., Lee, W.-C. & Oh, H.-T. The role of submarine groundwater discharge (SGD) in nutrient budgets of Gamak Bay, a shellfish farming bay, in Korea. *J. Sea Res.* **64**, 3, 224–230 (2010).
10. Shaw, R.D. & Prepas, E.E. Groundwater-lake interactions: I. Accuracy of seepage meter estimations of lake seepage. *J. Hydrol.* **119**, 105–120 (1990).
11. Das, K., Debnath, P., Duttagupta, S., Sarkar, S., Agrahari, S. & Mukherjee, A. Implication of submarine groundwater discharge to coastal ecology of the Bay of Bengal. *J. Earth Syst. Sci.* **129** (2020).
12. Hata, M., Sugimoto, R., Hori, M., Tomiyama, T. & Shoji, J. Occurrence, distribution and prey items of juvenile marbled sole Pseudopleuronectes yokohamae around a submarine groundwater seepage on a tidal flat in southwestern Japan. *J. Sea Res.* **111**, 47–53 (2016).
13. Freeze, R.A. & Cherry, J.A. Groundwater Prentice (Englewood Cliffs, Englewood Cliffs) (1979).
14. Burnett, W.C., Taniguchi, M. & Oberdorfer, J.A. Assessment of submarine groundwater discharge into the coastal zone. *J. Sea Res.* **46**, 109–116 (2001).
15. Porcelli, D. & Swarzenski, P.W. The behavior of U-and Th-series nuclides in groundwater. *Rev. Mineral. Geochem.* **52**, 1, 317–361 (2003).
16. Hwang, D.W., Kim, G., Lee, Y.-W. & Yang, H.-S. Estimating submarine inputs of groundwater and nutrients to a coastal bay using radium isotopes. *Mar. Chem.* **96**, 61–71 (2005).
17. Sawyer, A.H. et al. Continental patterns of submarine groundwater discharge reveal coastal vulnerabilities. *Science* **353** (2016).
18. Zhou, Y. Q., Sawyer, A. H., David, C. H. & Famiglietti, J. S. Fresh submarine groundwater discharge to the near-global coast. *Geophys. Res. Lett.* **46**, 5855–5863 (2019).
19. Luijendijk, E., Gleeson, T. & Moosdorf, N. Fresh groundwater discharge insignificant for the world's oceans but important for coastal ecosystems. *Nat Commun* **11**, 1260 (2020).

20. Destouni, G., Hannerz, F., Prieto, C., & Jarsjo, J. Small unmonitored near-coastal catchment areas yielding large mass loading to the sea. *Global Biogeochem. Cycles* **22**, GB4003 (2008).
21. Zhou, Y. Q., Befus, K. M., Sawyer, A. H. & David, C.H. Opportunities and challenges in computing fresh groundwater discharge to continental coastlines: A multimodel comparison for the United States Gulf and Atlantic Coasts. *Water Resour. Res.* **54**, 8363–8380 (2018).
22. Russo, A. A., Boutt, D. F., Munk, L. A. & Jenckes, J. Contribution of fresh submarine groundwater discharge to the Gulf of Alaska. *Water Resour. Res.* **59**, e2023WR034912 (2023).
23. Lee, Y.-W., Hwang, D.-W., Kim, G., Lee, W.-C. & Oh, H.-T. Nutrient inputs from submarine groundwater discharge (SGD) in Masan Bay, an embayment surrounded by heavily industrialized cities. *Korea. Sci. Total Environ.* **407**, 9, 3181–3188 (2009).
24. Hwang, D.-W., Lee, I.-S., Choi, M. & Kim, T.-H. Estimating the input of submarine groundwater discharge (SGD) and SGD-derived nutrients in Geoje Bay, Korea using 222 Rn-Si mass balance model. *Mar. Pollut. Bull.* **110**, 1, 119–126 (2016).
25. Kwon, H.K., Kang, H., Oh, Y.H., Park, S.R. & Kim, G. Green tide development associated with submarine groundwater discharge in a coastal harbor, Jeju, Korea. *Scientific Reports* **7** (2017).
26. Rodell, M., Houser, P.R., Jambor, U.E.A., Gottschalck, J., Mitchell, K., Meng, C-J., Arsenault, K., Cosgrove, B., Radakovich, J. & Bosilovich, M. The global land data assimilation system. *Bull. Am. Meteorol. Soc.* **85**, 381–394 (2004).
27. Kumar, S.V., Peters-Lidard, C.D., Tian, Y., Geiger, J., Houser, P.R. et al. LIS – an interoperable framework for high resolution land surface modeling. *Environ. Modell. Software* **21**, 1402–1415 (2006).
28. Jung, H.C. et al. Towards a soil moisture drought monitoring system for South Korea. *J. Hydrol.* **589** (2020).
29. Lee, K., Kang, D.H., Jung, H.C. et al. Toward a ground-based and long-term meteorological forcing dataset for South Korea. *Theor. Appl. Climatol.* **153**, 155–172 (2023).
30. Rodellas, V., Garcia-Orellana, J., Masque, P., Feldman, M. & Weinstein, Y. Submarine groundwater discharge as a major source of nutrients to the Mediterranean Sea. *Proc. Natl. Acad. Sci.* **112**, 3926-3930 (2015).
31. Chen, F., Janjicì, Z. & Mitchell, K. Impact of atmospheric surface-layer parameterizations in the new land-surface scheme of the NCEP Mesoscale Eta Model, Bound.-Lay. *Meteorol.* **85**, 391–421 (1997).
32. Chen, F., K., et al. Modeling of land-surface evaporation by four schemes and comparison with FIFE observations. *J. Geophys. Res.* **101**, 7251-7268 (2016).
33. Niu, G. Y. et al. The community Noah land surface model with multi-parameterization options (Noah-MP): 1. Model description and evaluation with local-scale measurements. *J. Geophys. Res.* **116**, D12109 (2011).
34. Yang, Z. L. et al. The community Noah land surface model with multiparameterization options (Noah-MP): 2. Evaluation over global river basins. *J. Geophys. Res.* **116**, D12110 (2011).
35. Best, M. J. et al. The Joint UK Land Environment Simulator (JULES), model description – Part 1: Energy and water fluxes. *Geosci. Model Dev.* **4**, 677–699 (2011).

555 36. Clark, D. B. et al. The Joint UK Land Environment Simulator (JULES), model
556 description – Part 2: Carbon fluxes and vegetation dynamics. *Geosci. Model Dev.*
557 **4**, 701–722 (2011).
558 37. Kumar, S. V.,Wang, S., Mocko, D.M., Peters-Lidard, C. D. & Xia, Y. Similarity
559 Assessment of Land Surface Model Outputs in the North American Land Data
560 Assimilation System, *Water Resour. Res.* **53**, 11, 8941–8965 (2017).
561 38. Guo, Z., Dirmeyer, P. A., Hu, Z.-Z., Gao, X., & Zhao, M. Evaluation of the second
562 global soil wetness project soil moisture simulations: 2. Sensitivity to external
563 meteorological forcing. *J. Geophys. Res.* **111**, D22S02 (2006).
564 39. Yoon. Y., Kumar, S. V. et al. Evaluating the uncertainty of terrestrial water budget
565 components over High Mountain Asia. *Front. Earth Sci*. **7**, 120 (2019).
566 40. Ghazal, K. A., Leta, O. T. & Dulai, H. Spatiotemporal estimation of fresh submarine
567 groundwater discharge across the coastal shorelines of Oahu Island, Hawaii. *Blue-*
568 *Green Syst.* **5**, 28-40 (2023).
569 41. Mazi, K., Koussis, A. D. & Destouni, G. Tipping points for seawater intrusion in
570 coastal aquifers under rising sea level. *Environ. Res. Lett.* **8**, 1 (2013).
571 42. Tapley, B., Bettadpur, S., Watkins, M. & Reigber, C. The gravity recovery and
572 climate experiment: mission overview and early results. *Geophys. Res. Lett.* **31**,
573 L09607 (2004).
574 43. Tamborski, J. J., Rogers, A. D., Bokuniewicz, H. J., Cochran, J. K. & Young, C. R.
575 Identification and quantification of diffuse fresh submarine groundwater discharge
576 via airborne thermal infrared remote sensing. *Remote Sens. Environ.* **171**, 202–217
577 (2015).
578 44. Yamazaki, D. et al. A high-accuracy map of global terrain elevations.
579 Geophys. Res. Lett. 44, 11 (2017).
580 45. Friedl, M., McIver, D., Hodges, J., Zhang, X., Muchoney, D., Strahler, A. et al.
581 Global land cover mapping from MODIS: algorithms and early results. *Remote Sens.*
582 *Environ.* **83**, 287–302 (2002).
583 46. Hengl, T., de Jesus, J., MacMillan, R., Batjes, N., Heuvelink, G., Ribeiro, E. et al.
584 SoilGrids1km - global soil information based on automated mapping. *PLoS ONE* **9**,
585 e105992 (2014).
586 47. Nguyen, P., Thorstensen, A., Sorooshian, S., Hsu, K., Aghakouchak, A. & Ashouri,
587 H., et al. Global Precipitation Trends across Spatial Scales Using Satellite
588 Observations. *Bull. Am. Meteorol. Soc.* **99**, 689–697 (2018).
589 48. Friedl, M. & Sulla-Menashe, D. MODIS/Terra+Aqua Land Cover Type Yearly L3
590 Global 500m SIN Grid V061 [Data set]. NASA EOSDIS Land Processes
591 Distributed Active Archive Center. Accessed 2023-09-27 from
592 https://doi.org/10.5067/MODIS/MCD12Q1.061 (2022).
593 49. Landerer, F. & Swenson, S. Accuracy of scaled GRACE terrestrial water storage
594 estimates. *Water Resour. Res.* **48**, W04531 (2012).
595

Acknowledgements

This research was supported by the Global-LAMP program (RS-2024-00442483) and the National Research Foundation of Korea (NRFK) grant (2021R1A2C100578013), funded by the Korean Government and Yonsei University Future-Leading Research Initiative (2023-22-0128).

Author contributions

H.J. and Y.Y. collaboratively designed the study. H.J. conducted the literature review and collected the datasets. Y.Y. performed the model runs and analysis. H.J. and Y.Y. jointly interpreted the results. Y.Y. created the visualizations. H.J. and Y.Y. wrote and revised the manuscript.

Competing interests

The authors declare no competing interests.

Table

Table 1. Average fresh submarine groundwater discharge (SGD) rates and net precipitation over the entire domain and each sub-region. The locations of the sub-regions are shown in Fig. 1. Ensemble averages from three land surface models are used for the regional analysis of fresh SGD rates along the Korean Peninsula.

	SGD (m^2/year)					Net Precipitation (kg^2/m)
Region	Noah v3.9	Noah-MP v4.0.1	JULES v5.5	Standard deviation	Ensemble average	
Entire domain	297	273	266	16.3	279	682
Pyongan	151	306	201	79.1	220	556
Hwangnam	199	331	253	66.4	261	513
Gyeonggi	490	264	275	127.4	343	856
Chungnam	506	483	468	19.1	486	658
Jeolla	330	288	254	38.1	291	834
Jeju	423	421	400	12.7	415	857
Gyeongnam	631	196	381	218.3	403	1105
Gyeongbuk	152	166	163	7.4	161	487
Gangwon	251	276	246	16.1	258	664
Hamgyong	56	189	141	67.4	128	285

Figures

Fig. 1. Map of fresh submarine groundwater discharge (SGD) rates along the coastline of the Korean Peninsula.

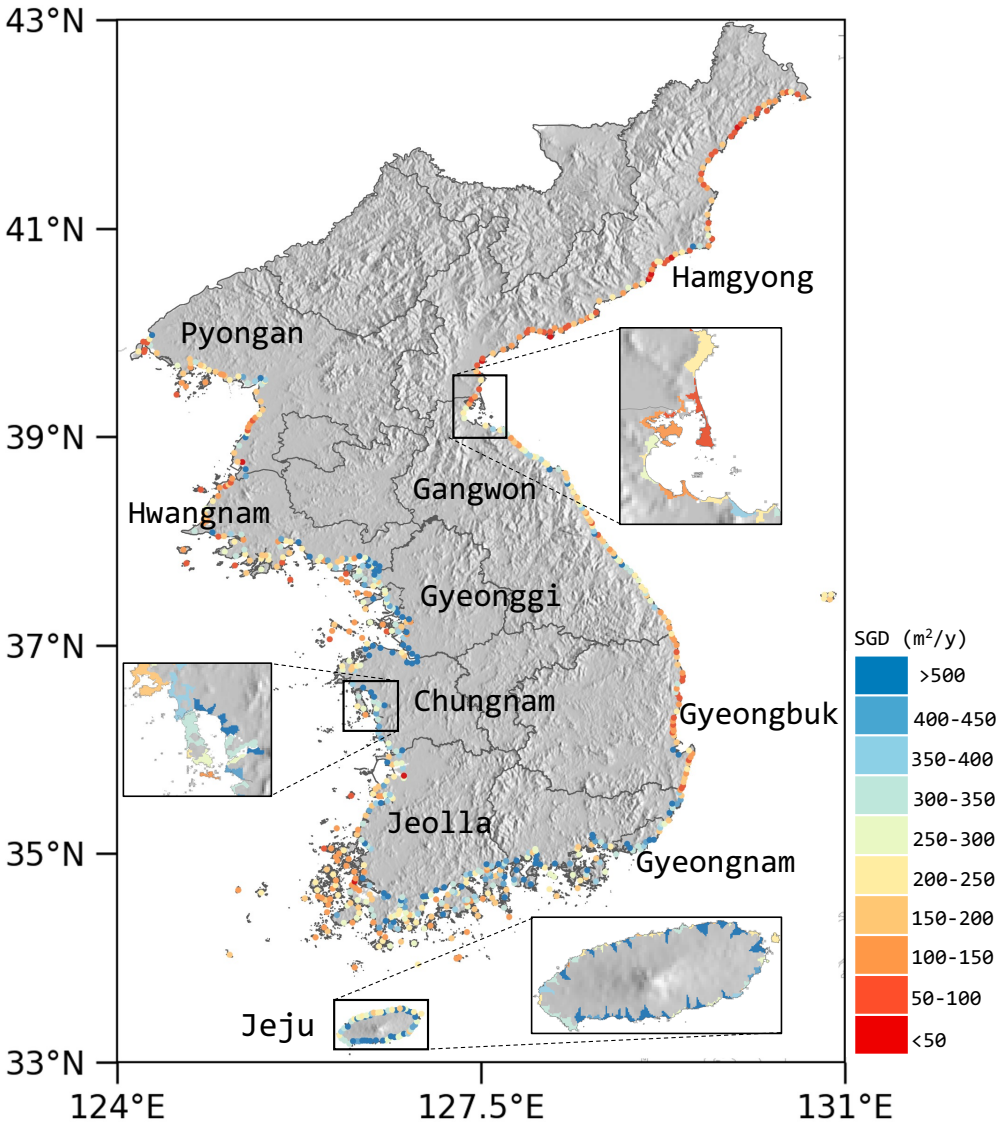

The average fresh SGD rate (m^2/year) is calculated by multiplying the average annual net recharge (m/year), obtained from three LSMs, by the drainage length (m) that is the coastal catchment area (km^2) divided by coastal length (km). Note that minor islands, mainly located in the west and south of Korean Peninsula, were excluded to prevent potential statistical biases. Information on all coastal catchments is provided in Supplementary Fig. 1. The sub-regions with the shaded relief map are shown as the background. As an example, three expanded views display coastal recharge zones colored according to the rate of fresh SGD.

Fig. 2. Spatial analysis of average fresh submarine groundwater discharge (SGD) rates, annual net precipitation, and coastal drainage length across regions.

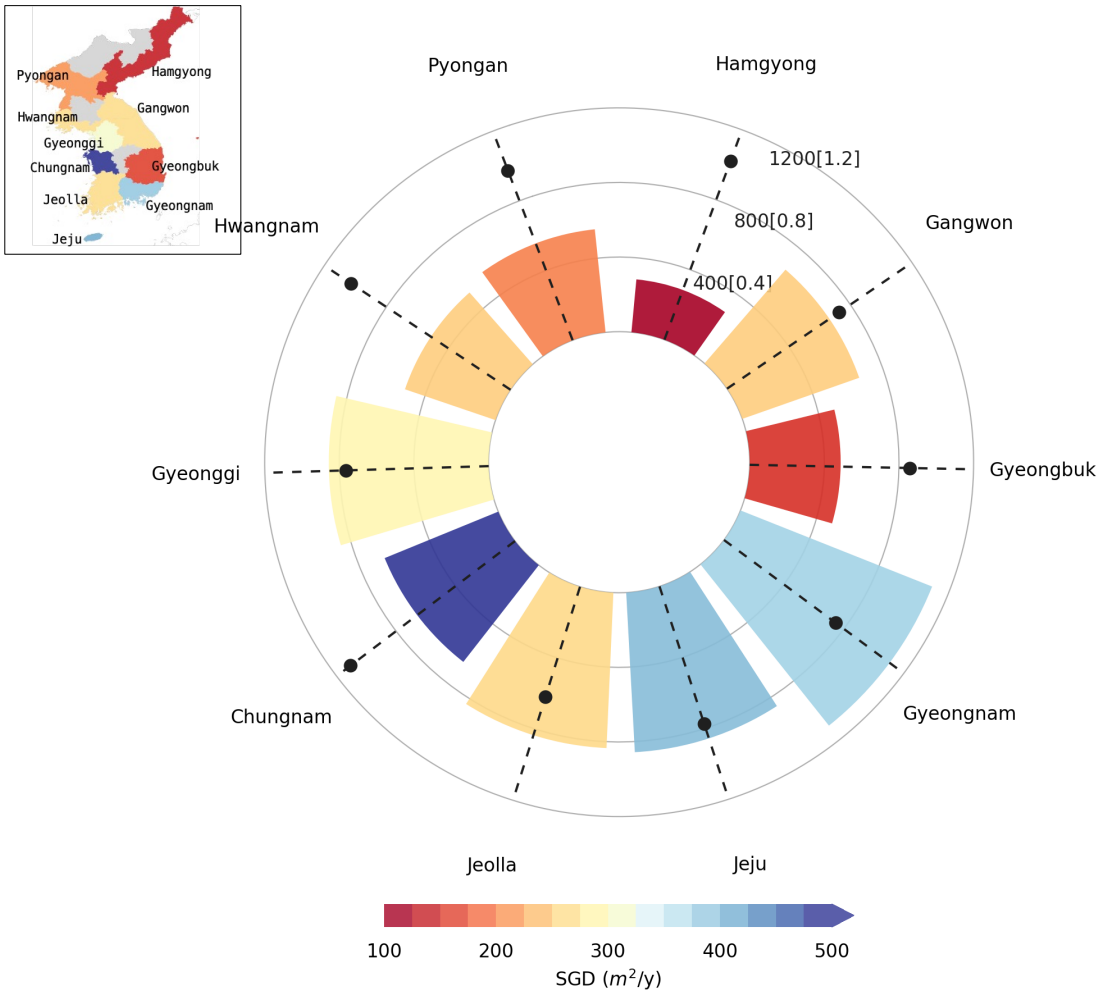

The color gradient corresponds to fresh SGD values. Net precipitation is represented by bar height, using a radial axis from 0 to 1200 kg/m^2. Dot height indicates coastal drainage length, with a radial axis ranging from 0 to 1.2 km. The box in upper left displays sub-region information, with colors corresponding to fresh SGD values.

Fig. 3. Trend analyses of fresh submarine groundwater discharge (SGD) and net precipitation rates using the Mann-Kendall trend test.

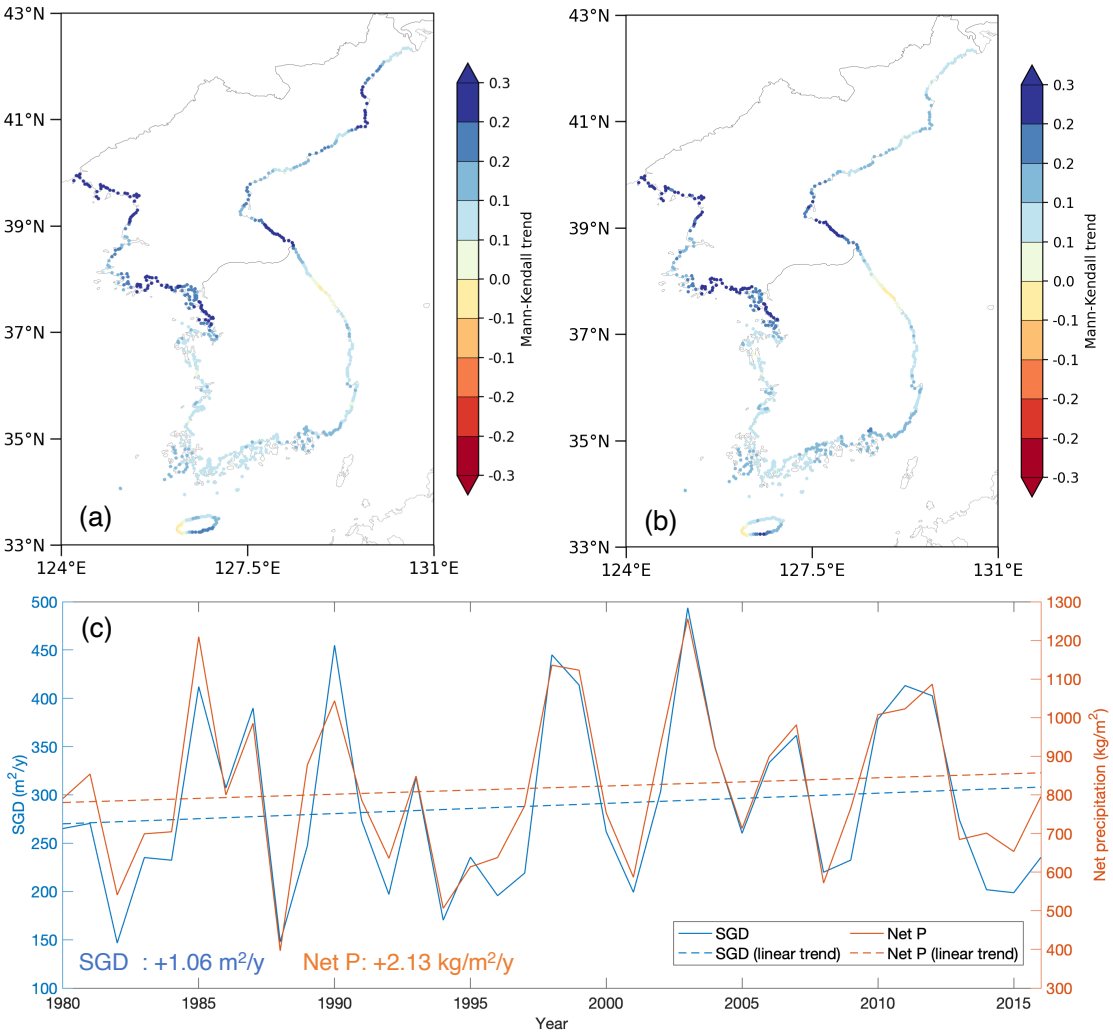

Maps illustrating the Mann-Kendall S-statistics for (a) SGD and (b) net precipitation (Net P) were generated across coastal catchments. (c) Time series analyses were performed to calculate the domain-averaged mean annual SGD and Net P for the years 1980-2016.

Fig. 4. Seasonal analyses of fresh SGD rates for the years 1980-2016.

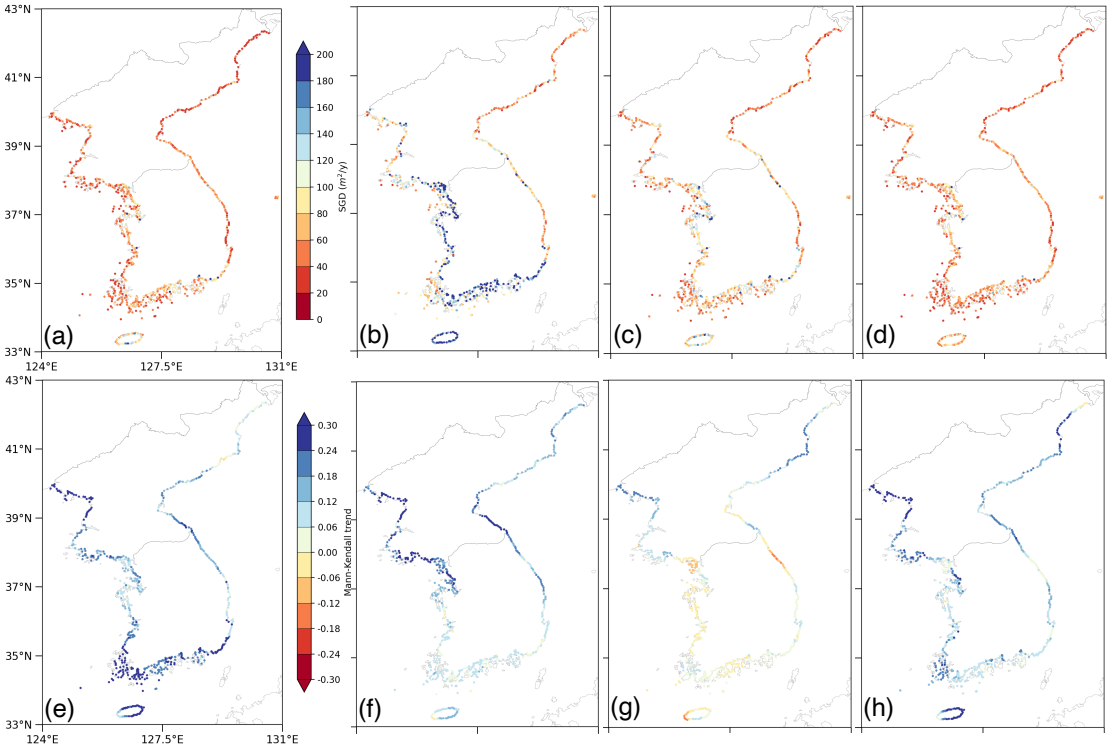

Maps for fresh SGD rates in (a) spring, (b) summer, (c) fall, and (d) winter. Concurrently, Mann-Kendall S-statistic estimates for (e) spring, (f) summer, (g) fall, and (h) winter were calculated to assess trends in the seasonal variations of fresh SGD rates.

Fig. 5. Assessment of coastal vulnerability of the Korean Peninsula.

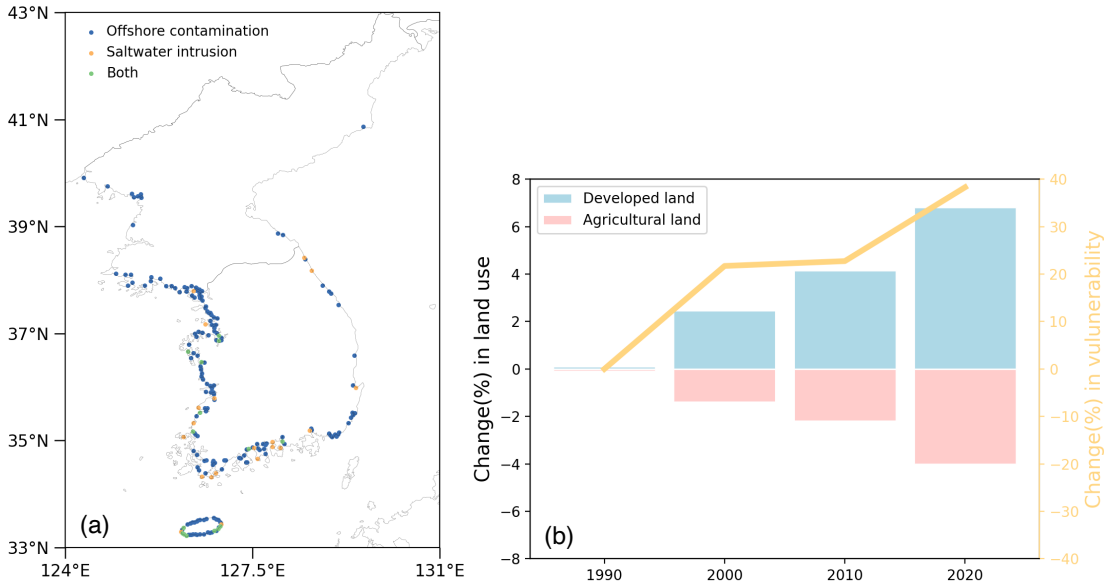

(a) Map of coastal vulnerability to offshore contamination and saltwater intrusion. Areas vulnerable to offshore contamination (indicated in dark blue) are identified where the rate of fresh SGD surpasses the average (297 m^2/year) and the usage of developed or agricultural land exceeds the average (38.7%). Vulnerability to saltwater intrusion (highlighted in orange) is identified in regions where low fresh SGD or high groundwater extraction may lead to complete saltwater invasion. Vulnerability to saltwater intrusion in the northern Korean Peninsula was not assessed due to limited available data. Coastal areas indicated in green are susceptible to both offshore contamination and saltwater intrusion. (b) The impact of decadal land use changes in the southern Korean Peninsula's coastal catchments on vulnerability to offshore contamination is explored. This assessment focuses exclusively on coastal catchment areas rather than on the entire country.

680 **Fig. 6. Time series of anomalies (mm) in total water storage (TWS) over coastal**
681 **catchments derived from the Gravity Recovery and Climate Experiment**
682 **(GRACE) products during 2002–2016**.

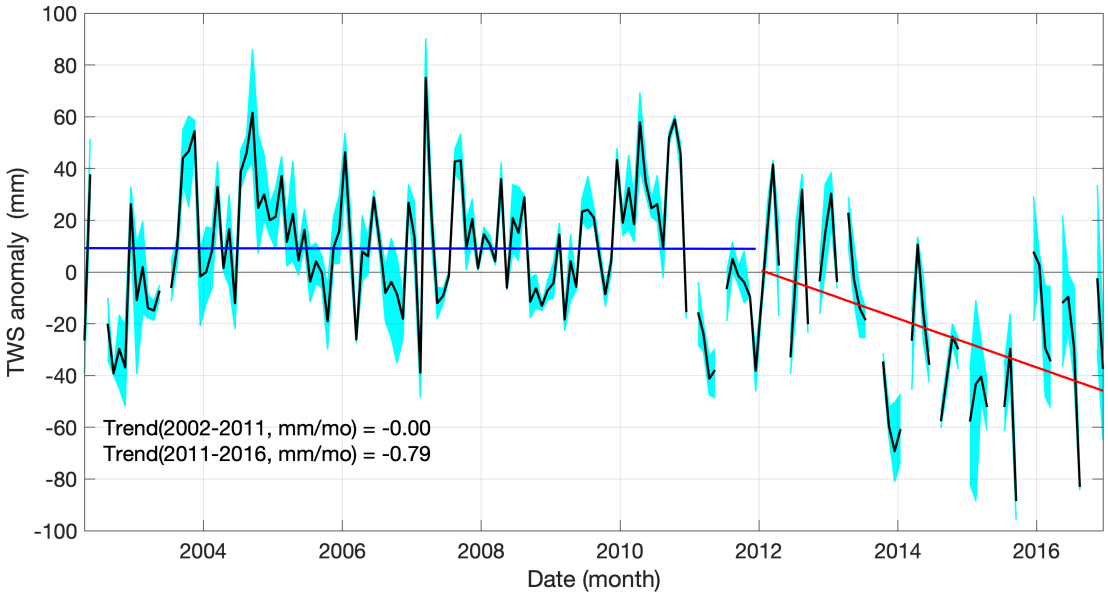

683

684 The cyan shading illustrates the variation in TWS anomalies among GRACE products.
685 The black line represents the mean of TWS anomalies. The blue and red lines show the
686 linear trends from 2002-2011 and 2011-2016, respectively.

687